Table I. Crystallization conditions.

Proteins (source)	Protein concentration (mg mL^{-1})	Protein buffer	Precipitant
Insulin (Bovine pancreas)	15	0.02 M Hydrochloric acid, pH 4.4	0.2 M Disodium hydrogen phosphate

Aldrich (lot 0001434060). The insulin crystals were prepared by a micro batch technique. Powdered insulin was dissolved in 0.02 M hydrochloric acid at pH 4.4 (Wako) to an insulin concentration of 30 mg/mL and filtered through a 0.45 μm pore filter (Advantec Dismic-03cp). Disodium hydrogen phosphate (Wako) was dissolved in water to a concentration of 0.4 M as the precipitant (Table I). The gel laid on the batch bottom was Agarose SP (SeaPlaque® Agarose Lonza) mixed with water to a concentration of 2.0% w/v.[18] The micro-stirring technique was accomplished using a rotary shaker.[11] The insulin crystals were grown at 293 K.

2.2 Crystallization with the stirring technique

First, the insulin solution was adjusted to 15 mg/mL by 0.2 M disodium hydrogen phosphate. Second, 4 μL of the crystallization drops were dispensed onto an Imp@ct plate (Hampton Research) and the drops were stirred with a rotary shaker until the crystals on the plates were mounted on cryoloops for X-ray diffraction (XRD). In this research, the rotation speeds were set at 0, 15, 30, 50, 75, and 100 rpm. Each plate was stirred at the respective speeds.

2.3 Crystallization with the high-concentrated hydrogel

First, Agarose SP was dispensed onto an Imp@ct plate and placed at 277 K for over 12 h. Second, 2 μL protein drops were dispensed onto the gel and allowed to stand for 5 min for the drops to pass into the gel. Third, 2 μL of the precipitant was dispensed onto the protein drop.

The crystals grew at the interface between the hydrogel and the solution [Figs. 2(a) and 2(b)]. We defined these crystals as the "gel-interface crystal". We also defined the crystals grown in the solution without hydrogel as "solution-grown crystal". In this work, we selected the insulin crystals with morphologies almost the same as that shown in Fig. 2(a). Gel-interface crystals did not detach from the hydrogel when they were mounted on nylon loops. This indicated that the crystals were partially incorporated into the hydrogel and fixed on it.

2.4 XRD data collection

Insulin crystals were observed with optical microscopy before the XRD experiment. We selected single crystals without any cracks. Moreover, the size of the crystals was limited to within 170 to 230 μm in the direction of the arrow in Fig. 2(c), because the size of the insulin crystals can affect the XRD intensity. Diffraction data from the insulin crystals were collected on a Rigaku R-AXIS IV^{++} imaging plate. Cu Kα radiation was produced using a rotating anode generator operating at 40 kV and 30 mA. The crystal-to-detector distance was set at 90 mm. Two hundred flames were collected in the 2θ range from 0 to 200°. The X-ray exposure time was 6 s. XRD experiments were performed under liquid nitrogen-cooled conditions at 100 K. The crystals were mounted in nylon loops, soaked for 3 min in 30% glycerol (Wako), 0.3 M disodium hydrogen phosphate and then frozen by rapidly submerging them in liquid nitrogen. All data was processed with iMosflm (version 1.0.5).[19] The processed images were merged and scaled with scala of the ccp4i suite (version 6.2.0).[20] Three diffraction data sets were collected under each condition.

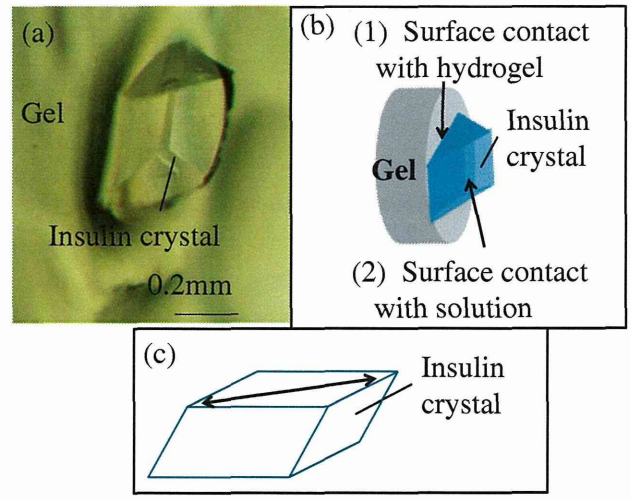

Fig. 2. (Color online) (a) Photograph of an insulin crystal grown at the interface between the hydrogel and the solution (gel-interface crystal) and (b) schematic illustration of gel-interface insulin crystal. (c) A schematic image of insulin crystal. The solid arrow is the measurement point for each crystal size.

2.5 Observation of the crystal surface

Laser confocal microscopy combined with differential interference contrast microscopy (LCM–DIM) was employed to observe the elementary steps of the insulin crystals. Details of LCM–DIM are described in Refs. 21–24. 100 LCM–DIM images (Fig. 6) were acquired with a time-lapse of 20 s between each image. The total observation time ranged from 0 to 33 min. The observation cell was set on a temperature-controlled stage, which kept temperatures at ±0.1 K, using Peltier elements. The step velocity was measured with the average growth/dissolution rate of 2D islands/etch pits ($N = 1$ to 5).

3. Results and discussion

The insulin crystals grown with the solution stirring technique were evaluated with a temperature factor determined by the slopes of the Wilson Plots.[25,26] The solubility of the insulin crystals grown at the interface between the hydrogel and the solution (gel-interface crystals) was then tested and compared to the regular solution-grown crystals (solution-grown crystals). In Ref. 13, a lysozyme crystal grown in a hydrogel started to dissolve at a temperature 2 K higher than the crystal grown in solution. This is evidence that the hydrogel-grown crystals have improved environmental stability (e.g., stability to temperature change) than those grown in solution. The crystal etching strategy and step velocity measurement were applied to determine the difference in the crystal dissolving point between the gel-interface and the solution-grown crystals. The solubility of the gel-interface crystals was then evaluated.

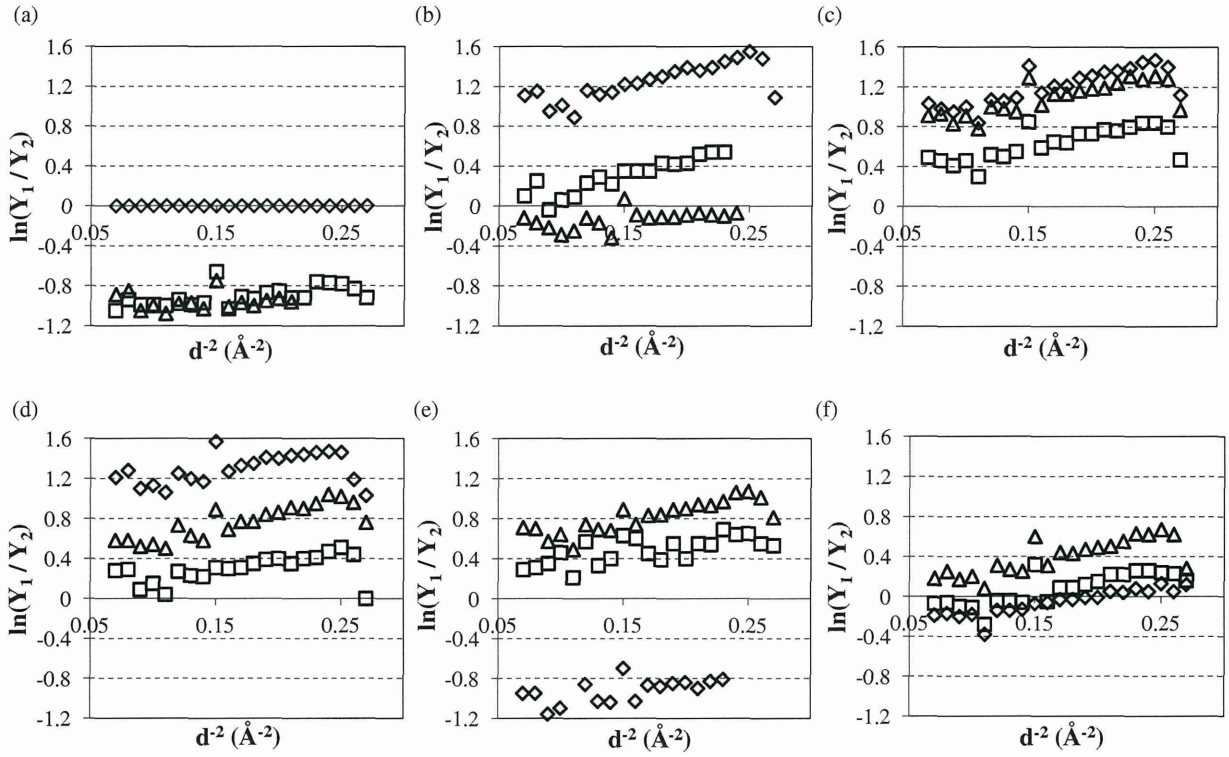

Fig. 3. Wilson Plots of solution-grown crystals grown with the solution stirring technique at 0 (a), 15 (b), 30 (c), 50 (d), 75 (e), and 100 rpm (f). Three different symbols (rhombus, square, and triangle) indicate three different experiments at each rotation speed.

3.1 Measurement of average temperature factor

The quality of insulin crystals grown with the solution stirring technique was investigated by the average temperature factor.[25,26] The iMosflm program was used for the evaluation of the crystals.[19] The resolution range was limited to R-sym < 0.35 and $I/\sigma > 2.5$.

The Wilson Plot is described by

$$\ln|Y| = \ln|k| - 2B \cdot \sin^2\theta/\lambda^2, \quad (1)$$

where Y is the S/N ratio of diffraction intensity, k the scale factor, B the average temperature factor, θ Bragg angle, λ the X-ray wavelength, and resolution is $d = \lambda/2\sin\theta$.

Equation (1) is transformed into Eq. (2):[25]

$$\ln(Y_1/Y_2) = \ln(k_1 - k_2) - 2(B_1 - B_2) \cdot \sin^2\theta/\lambda^2, \quad (2)$$

In Eq. (2) the crystal for evaluation is defined as "1", and the crystal for reference (a standard crystal) is defined as "2". One of the insulin crystals grown without stirring was used as the standard crystal. In this work, the difference between temperature factors [$B_1 - B_2$ in Eq. (2)], which corresponds to the slope of each plot, was used to evaluate the quality of the insulin crystals. Figure 3 shows graphs of the Wilson Plots [Eq. (2)] of solution-grown insulin crystals grown with or without the solution stirring. The horizontal axis is d^{-2} ($= 4\sin^2\theta/\lambda^2$), and the vertical axis is $\ln(Y_1/Y_2)$. The slope of these graphs indicates the quality of the crystals compared with the reference crystal. The solution flow rates ranged from 0 to 100 rpm, for the set point of the rotary shakers. Generally, a positive slope indicates that the crystal has a higher quality than the reference crystal, and a negative slope indicates that the crystal has a lower quality than the reference crystal. In Fig. 3, it can be seen that the slopes are almost 0 at 0 rpm. In contrast, the slopes are positive from 15 to 100 rpm. This indicates that the quality of insulin crystals was improved by the effect of the solution stirring technique.

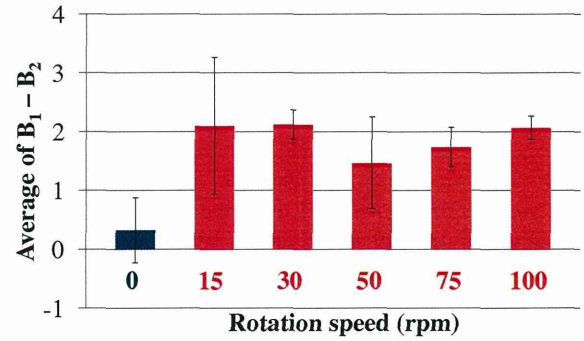

Fig. 4. (Color online) The average of $(B_1 - B_2)$ in the solution-grown crystals. $(B_1 - B_2)$ is the difference of temperature factors between a standard crystal and a crystal for evaluation.

For a better understanding, the averages of $(B_1 - B_2)$ obtained from the slopes of the Wilson Plots were plotted (Fig. 4). The average of $(B_1 - B_2)$ of crystals grown with the solution stirring technique was clearly higher than that of crystals grown without the solution stirring technique. However, no dependency between the average of $(B_1 - B_2)$ and the rotation speed (15–100 rpm) was apparent. These results suggest two possibilities: either a slight solution flow is enough for the improvement of protein crystal growth, or there may exist a more suitable solution flow rate for growing

high quality protein crystals at a faster solution flow rate. What is apparent is that solution flow has positive effects on protein crystal growth in the range of 15–100 rpm. Additional experiments at faster solution flow rates are an attractive future study for the advancement of the crystal growth technique with solution flow.

The insulin solution contained impurities with molecular weights lower than that of insulin [see the online supplementary material (available at http://stacks.iop.org/JJAP/53/065502/mmedia)]. Crystal quality can be strongly affected by impurities in the protein solution, therefore the behavior of the impurities at the surface of the growing crystals must also be considered. Parameter K, the ratio of the impurity concentration in the crystal to its average concentration in the mother solution, makes it easy to consider the behavior of such impurities.[27] According to Refs. 27 and 28, solution stirring is probably effective in the presence of impurities with a $K < 1$. Furthermore, if the appropriate solution stirring velocity is selected, the stirring technique has the possibility to also be effective in the presence of impurities that are easily incorporated into the crystals.[29,30] The results indicate that the incorporation of impurities was effectively reduced by the solution stirring with the rotary shaker, which enhances the alignment of the crystal lattice and protein molecule.[28] The results also indicate that the K of the main impurity contained in insulin solution was possibly smaller than 1.

3.2 Evaluation of the environmental stability of insulin crystals

The solubility of the gel-interface insulin crystals was tested and compared to the solution-grown crystals. The dissolution point of each crystal was determined by the observation of step advancement/retreat on the crystal surfaces using LCM–DIM at a temperature range from 293 to 304 K. For the observation of the gel-interface crystal surface, the surface facing the solution side was selected. [see (2) in Fig. 2(b)]. The surface surrounded by hydrogel [see (1) in Fig. 2(b)] was expected to dissolve slower than that not in contact with the hydrogel, because the hydrogel inhibits the diffusion of solute. This may be the main rate-limiting factor. Such an observation makes the discussion complicated. The observation of the surface facing the solution will provide a precise dissolution point of the gel-interface crystal, and enable the solubility of the insulin crystals to be evaluated.

One to five 2D islands or etch pits of a gel-interface crystal and a solution-grown crystal were selected for measurement points, and the growth or dissolution rate of the same direction steps were measured. In the case of etch pits, shallow etch pits were selected because the step movement can be strongly affected by step density.[31] Figure 5 shows the advancement/retreat velocity of the steps depending on the temperature. The differences in growth rates between gel-interface and solution-grown crystals were not apparent thus are considered to have the same tendency. However, apparent differences in the dissolution point can be seen. The dissolution point was 300 K in the case of a solution-grown crystal. In contrast, the temperature was 302 K in the case of a gel-interface crystal, 2 K higher than that of a solution-grown crystal.

Figure 6 shows the surfaces of a solution-grown crystal [(a) and (c)] and a gel-interface crystal [(b) and (d)]. Figures 6(a) and 6(b) are images taken just after the temperature was set to 301 K, and Figs. 6(c) and 6(d) are images after 33 min at 301 K. At 301 K, the surface of the solution-grown crystal was dissolved and the 2D islands became rounded and smaller [Figs. 6(a) and 6(c)]. That of the gel-interface crystal, in contrast, showed no change, and the edges of the 2D islands remained sharp [Figs. 6(b) and 6(d)]. The surface changes of both types of crystals at 301 K are strong corroboration of the data sets in Fig. 5.

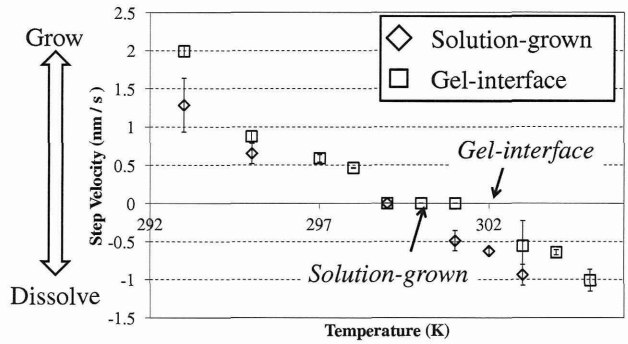

Fig. 5. Plot of the growth or dissolution rate of the insulin crystals. The solution-grown crystal started dissolving at 300 K. The gel-interface crystal started dissolving at 302 K.

According to Ref. 32, if agarose gel exists around a crystal, the growth rate is affected and there should be differences, i.e., reduction or promotion of the step velocity, that would strongly depend on the impurities in a solution. Considering the growth rate in Fig. 6, no such effects as described in Ref. 32 were observed. Thus, the surface of the gel-interface crystal facing toward the solution was certainly not covered with agarose gel. Additionally, the dependency of growth/dissolution velocity on temperature was clearly intrinsic to the gel-interface crystals. The higher tolerance for temperature changes of gel-interface crystals was consistent with the crystals grown in the hydrogels reported in Ref. 13. Crystals grown in hydrogel have an improved environmental stability because the gel fiber irrupts into the crystal,[13,33] which may support the crystal structure. Furthermore, the results clearly indicate that if a crystal incorporates agarose gel, the gel can support the crystals and their environmental stability is improved (Fig. 7). This provides much more variety in gel applications, and strongly indicates that our new concept of a crystal growth technique, the on-gel stirring technique, has a high possibility of obtaining high-quality crystals with improved environmental stability.

3.3 Application of the on-gel stirring technique to the insulin crystal growth

We showed the effectiveness of solution stirring on crystal growth by the relative Wilson plot. Solution flow in the range of 15–100 rpm has positive effects on protein crystal growth. The environmental stability of a protein crystal is improved when a crystal is grown at a gel-solution interface. To obtain the both effects, we grew an insulin crystal at a gel-solution interface with a solution stirring which range of 100 rpm. We also grew an insulin crystal at a gel solution interface without a solution stirring as a reference. Figures 8(a) and 8(b) are the insulin crystals after soaking for 3 min in 30% glycerol. There

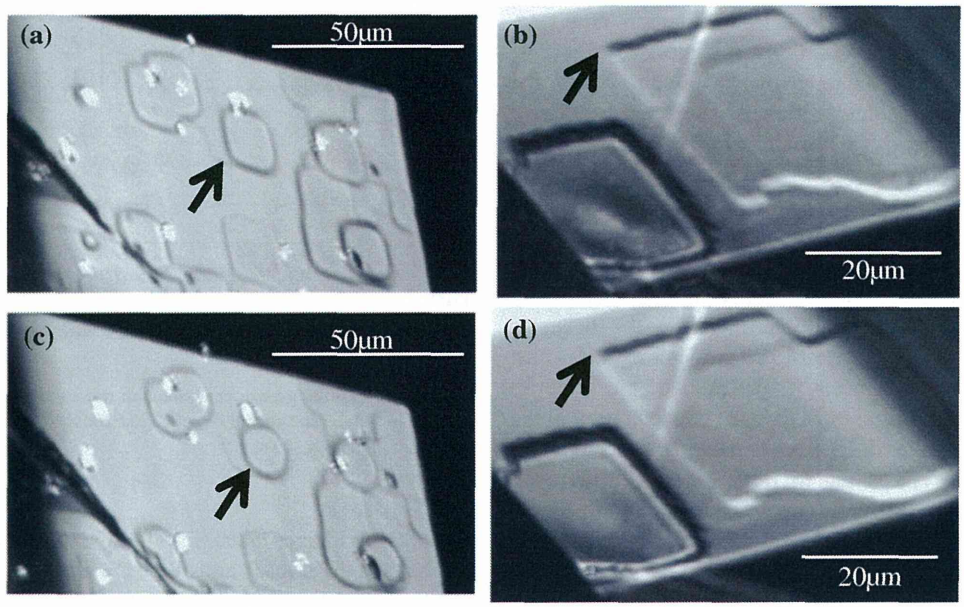

Fig. 6. Surface changes of solution-grown (a, c) and gel-interface (b, d) insulin crystals. The time change for (c) and (d) is 33 min after setting temperature to 301 K. The solution-grown crystal was dissolved (a, c). The gel-interface crystal showed no change (b, d).

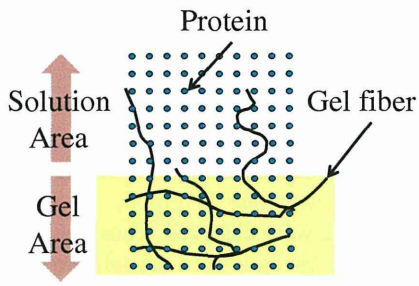

Fig. 7. (Color online) Schematic illustration of the irruption of gel fiber into the gel-interface crystal.

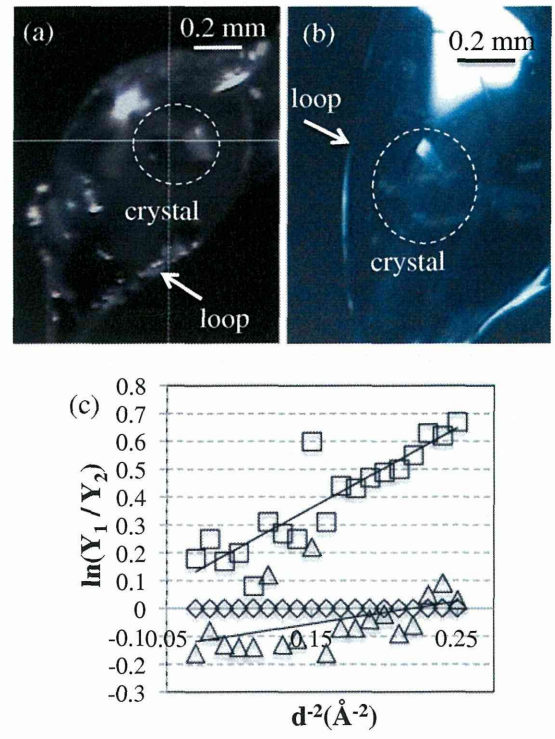

Fig. 8. (Color online) Images of the on-gel crystal grown at 0 rpm (a), and the on-gel crystal grown at 100 rpm (b). (c) Relative Wilson plots. The rhomboid symbol corresponds to the data of the standard crystal (same as the standard crystal of Fig. 3). The triangle symbol is the data of an on-gel crystal without stirring, and the square symbol is the data of an on-gel crystal at stirring of 100 rpm.

were no visible damages in the crystal. The crystal quality was also measured by XRD experiment, and evaluated with a temperature factor determined by the slopes of the Wilson Plots. All of the experimental parameters are same as those of the former paragraph. The standard crystal was same as Fig. 3 (a solution grown crystal without stirring). Figure 8(c) is the Wilson plot of the three insulin crystals. The rhomboid symbol corresponds to the data of the standard crystal. The triangle symbol is the data of an on-gel crystal without stirring, and the square symbol is the data of an on-gel crystal at stirring of 100 rpm. The temperature factor (correspond to the slope of the plot) of an on-gel crystal without stirring was 0.8, which indicate better quality than the standard crystal. Furthermore the temperature factor of an on-gel crystal with 100 rpm stirring was about 2.9, which was higher value than the average temperature factors of solution grown crystals with solution stirring (see Fig. 4). These results indicate that the newly developed on-gel stirring technique is a very effective and promising way to obtain a protein crystal suitable for XRD diffraction measurement.

4. Conclusions

We evaluated crystals grown with the solution stirring technique by the average difference between temperature factors determined by the slopes of the Wilson Plots [Eq. (2)]. Higher-quality insulin crystals could be obtained under the stirred environment.

The environmental stability of the insulin crystals grown at the interface between the hydrogel and the solution for temperature change was also tested. The dissolution point of a gel-interface crystal was 302 K, which was 2 K higher than that of a solution-grown crystal. This result showed that agarose gel can support the crystals and improve their environmental stability.

To realize the solution stirring effect and the gel effect, we combined the two techniques and grew an insulin crystal using it. The crystal quality was evaluated by the relative Wilson plots and the calculated temperature factor showed that the on-gel stirring crystal has higher quality than solution-grown crystals with stirring and on-gel crystals without stirring.

These results confirm that the newly developed on-gel stirring technique has a greater possibility of obtaining high-quality crystals with improved environmental stability. This novel protein crystallization technique, which requires only simple settings and a simple procedure, will accelerate structural genomics and subsequent structure-based drug discoveries.

Acknowledgments

This work was supported by JSPS KAKENHI Grant Number 23360011 to Y.M., and partly supported by the Osaka University Program for the Support of Networking among Present and Future Researchers to M.M. Also it was partly supported by JSPS KAKENHI Grant Numbers 24656006, 24680050, and 24106505 to H.Y.Y.

1) G. E. O. Borgstahl, A. Vahedi-Faridi, J. Lovelace, H. D. Bergstahl, and E. H. Snell, Acta Crystallogr., Sect. D **57**, 1204 (2001).
2) K. Kitano, R. Sasaki, T. Nogi, T. A. Fukami, A. Nakagawa, K. Miki, and I. Tanaka, J. Cryst. Growth **210**, 819 (2000).
3) M. Ataka, E. Katoh, and N. I. Wakamiya, J. Cryst. Growth **173**, 592 (1997).
4) S. Sakurazawa, T. Kubota, and M. Ataka, J. Cryst. Growth **196**, 325 (1999).
5) S. X. Lin, M. Zhou, A. Azzi, G. I. Xu, N. I. Wakamiya, and M. Ataka, Biochem. Biophys. Res. Commun. **275**, 274 (2000).
6) T. Sato, Y. Yamada, S. Saijo, T. Hori, R. Hirose, N. Tanaka, G. Suzuki, K. Nakajima, N. Igarashi, M. Tanaka, and Y. Matsuura, Acta Crystallogr., Sect. D **56**, 1079 (2000).
7) L. Wang, C. Zhong, and N. I. Wakayama, J. Cryst. Growth **237**, 312 (2002).
8) B. Cudney, S. Patel, and A. McPherson, Acta Crystallogr., Sect. D **50**, 479 (1994).
9) J. M. García-Ruiz and A. Moreno, Acta Crystallogr., Sect. D **50**, 484 (1994).
10) D. W. Zhu, B. Lorber, C. Sauter, J. D. Ng, P. Beans, C. Grimellec, and R. Giege, Acta Crystallogr., Sect. D **57**, 552 (2001).
11) H. Adachi, K. Takano, M. Yoshimura, Y. Mori, and T. Sasaki, Jpn. J. Appl. Phys. **42**, L314 (2003).
12) S. Sugiyama, M. Hirose, N. Shimizu, M. Niiyama, M. Maruyama, G. Sazaki, R. Murai, H. Adachi, K. Takano, S. Murakami, T. Inoue, Y. Mori, and H. Matsumura, Jpn. J. Appl. Phys. **50**, 025502 (2011).
13) S. Sugiyama, H. Hasenaka, M. Hirose, N. Shimizu, T. Kitatani, Y. Takahashi, H. Adachi, K. Takano, S. Murakami, T. Inoue, Y. Mori, and H. Matsumura, Jpn. J. Appl. Phys. **48**, 105502 (2009).
14) H. Hasenaka, S. Sugiyama, M. Hirose, N. Shimizu, T. Kitatani, Y. Takahashi, H. Adachi, K. Takano, S. Murakami, Y. Mori, T. Inoue, and H. Matsumura, J. Cryst. Growth **312**, 73 (2009).
15) H. Matsumura, S. Sugiyama, M. Hirose, K. Kakinouchi, M. Maruyama, H. Adachi, R. Murai, K. Takano, S. Murakami, Y. Mori, and T. Inoue, J. Synchrotron Radiat. **18**, 16 (2011).
16) K. Tanabe, M. Hirose, R. Murai, S. Sugiyama, N. Shimizu, M. Maruyama, Y. Takahashi, H. Adachi, K. Takano, S. Murakami, Y. Mori, E. Mizohata, T. Inoue, and H. Matsumura, Appl. Phys. Express **2**, 125501 (2009).
17) S. Sugiyama, M. Maruyama, G. Sazaki, M. Hirose, H. Adachi, K. Takano, S. Murakami, T. Inoue, Y. Mori, and H. Matsumura, J. Am. Chem. Soc. **134**, 5786 (2012).
18) S. Sugiyama, K. Tanabe, M. Hirose, T. Kitatani, H. Hasenaka, Y. Takahashi, H. Adachi, K. Takano, S. Murakami, Y. Mori, T. Inoue, and H. Matsumura, Jpn. J. Appl. Phys. **48**, 075502 (2009).
19) T. G. G. Battye, L. Kontogiannis, O. Johnson, H. R. Powell, and A. G. W. Leslie, Acta Crystallogr., Sect. D **67**, 271 (2011).
20) M. D. Winn, C. C. Ballard, K. D. Cowtan, E. J. Dodson, P. Emsley, P. R. Evans, R. M. Keegan, E. B. Krissinel, A. G. W. Leslie, A. McCoy, S. J. McNicholas, G. N. Murshudov, N. S. Pannu, E. A. Potterton, H. R. Powell, R. J. Read, A. Vagin, and K. S. Wilson, Acta Crystallogr., Sect. D **67**, 235 (2011).
21) G. Sazaki, T. Matsui, K. Tsukamoto, N. Usami, T. Ujihara, K. Fujiwara, and K. Nakajima, J. Cryst. Growth **262**, 536 (2004).
22) G. Sazaki, K. Tsukamoto, S. Yai, M. Okada, and K. Nakajima, Cryst. Growth Des. **5**, 1729 (2005).
23) A. E. S. Van Driessche, G. Sazaki, F. Otalora, F. M. Gonzalez-Rico, P. Dold, K. Tsukamoto, and K. Nakajima, Cryst. Growth Des. **7**, 1980 (2007).
24) A. E. S. Van Driessche, F. Otalora, G. Sazaki, M. Sleutel, K. Tsukamoto, and J. A. Gavira, Cryst. Growth Des. **8**, 4316 (2008).
25) S. Arai, T. Chatake, N. Suzuki, H. Mizuno, and N. Niimura, Acta Crystallogr., Sect. D **60**, 1032 (2004).
26) N. Niimura and A. Podjarny, *Neutron Protein Crystallography* (Oxford University Press, Oxford, U.K., 2011) p. 64.
27) F. Otálora, J. A. Gavira, J. D. Ng, and J. M. García-Ruíz, Prog. Biophys. Mol. Biol. **101**, 26 (2009).
28) A. A. Chernov, J. Struct. Biol. **142**, 3 (2003).
29) M. Maruyama, H. Kawahara, G. Sazaki, S. Maki, Y. Takahashi, H. Y. Yoshikawa, S. Sugiyama, H. Adachi, K. Takano, H. Matsumura, T. Inoue, S. Murakami, and Y. Mori, Cryst. Growth Des. **12**, 2856 (2012).
30) P. G. Vekilov, B. R. Thomas, and F. Rosenberger, J. Phys. Chem. B **102**, 5208 (1998).
31) M. Maruyama, K. Tsukamoto, G. Sazaki, Y. Nishimura, and P. G. Vekilov, Cryst. Growth Des. **9**, 127 (2009).
32) A. E. S. Van Driessche, F. Otálora, J. A. Gavira, and G. Sazaki, Cryst. Growth Des. **8**, 3623 (2008).
33) J. A. Gavira and J. M. Garcia-Ruiz, Acta Crystallogr., Sect. D **58**, 1653 (2002).

Chem Soc Rev

TUTORIAL REVIEW

View Article Online
View Journal | View Issue

Laser ablation for protein crystal nucleation and seeding

Cite this: *Chem. Soc. Rev.*, 2014, 43, 2147

Hiroshi Y. Yoshikawa,*[ab] Ryota Murai,[c] Hiroaki Adachi,[bd] Shigeru Sugiyama,[b] Mihoko Maruyama,[b] Yoshinori Takahashi,[b] Kazufumi Takano,[de] Hiroyoshi Matsumura,[bd] Tsuyoshi Inoue,[bd] Satoshi Murakami,[df] Hiroshi Masuhara[g] and Yusuke Mori[bd]

Received 1st July 2013

DOI: 10.1039/c3cs60226e

www.rsc.org/csr

With the recent development in pulsed lasers with ultrashort pulse widths or wavelengths, spatially precise, low-damage processing by femtosecond or deep-UV laser ablation has shown promise for the production of protein single crystals suitable for X-ray crystallography. Femtosecond laser processing of supersaturated solutions can shorten the protein nucleation period or can induce nucleation at low supersaturation, which improves the crystal quality of various proteins including membrane proteins and supra-complexes. In addition to nucleation, processing of protein crystals by femtosecond or deep-UV laser ablation can produce single crystalline micro- or macro-seeds without deterioration of crystal quality. This tutorial review gives an overview of the successful application of laser ablation techniques to nucleation and seeding for the production of protein single crystals, and also describes the advantages from a physico-chemical perspective.

Key learning points

(1) Protein crystal nucleation and seeding by laser ablation enable the production of high-quality protein single crystals that are necessary for X-ray crystallography.

(2) Use of lasers with ultrashort pulse widths or wavelengths allows spatially precise, low-damage processing of protein solutions and crystals *via* specific ablation processes (*e.g.* photomechanical and photochemical).

(3) Processing of supersaturated solutions by femtosecond laser ablation can induce protein nucleation at low supersaturation, which results in the growth of high-quality single crystals.

(4) Processing of protein crystals by femtosecond or deep-UV laser ablation can produce single crystalline micro- or macro-seeds without deterioration of crystal quality.

1. Introduction

The three-dimensional (3D) structures of proteins have been attracting considerable attention because of a fundamental interest in the many biological processes involving proteins, as well as for structure-based drug design.[1] X-ray diffraction (XRD) of protein single crystals is the most widely used technique for determining the 3D structures with atomic resolution. However, protein crystallization, which involves nucleation and crystal growth, remains a major bottleneck in the structural determination process.[2] Although automated instrumentation has been developed to carry out high throughput screening of various crystallization conditions,[3] crystallographers often face difficulty in determining which set of conditions provide high-quality protein single crystals suitable for XRD. There are also many types of recalcitrant proteins (*e.g.*, membrane proteins) which are particularly difficult to crystallize because of their weak interactions and instability. Moreover, to improve the understanding of protein functions, structural determination at higher resolution is needed, even for proteins whose structures have already been deposited in the Protein Data Bank (PDB).

[a] *Department of Chemistry, Saitama University, Shimo-okubo 255, Sakura, Saitama 338-8570, Japan. E-mail: hiroshi@mail.saitama-u.ac.jp*
[b] *Graduate School of Engineering, Osaka University, Yamadaoka 2-1, Suita, Osaka 565-0871, Japan*
[c] *Graduate School of Energy Science, Kyoto University, Yoshida-Honmachi, Sakyo-ku, Kyoto, 606-8501, Japan*
[d] *SOSHO Inc., 313 Photonics Center Bldg., Yamadaoka 2-1, Suita, Osaka 565-0871, Japan*
[e] *Graduate School of Life and Environmental Sciences, Kyoto Prefectural University, 1-5 Hangi-cho, Shimogamo, Sakyo-ku, Kyoto 606-8522, Japan*
[f] *Graduate School of Bioscience and Biotechnology, Tokyo Institute of Technology, Nagatsuka 4259, Midori-ku, Yokohama, Kanagawa, 226-8501, Japan*
[g] *Department of Applied Chemistry and Institute of Molecular Science, National Chiao Tung University, Hsinchu 30010, Taiwan*

For example, X-ray resolution better than 1.0 Å may enable the assignment of hydrogen atoms, giving a more detailed view of protein hydration and enzymatic functions. However, a very limited number (~400) of protein structures have been solved beyond 1.0 Å resolution with respect to total number (~80 000) of protein structures in the PDB (as of June 2013). Thus innovation in protein crystallization techniques is necessary for accelerated advancement in the structural biology field.

The most conventional methods for protein crystallization are vapor diffusion (evaporation) and batch techniques, which basically adjust supersaturation of a protein solution by alternations in crystallization parameters such as concentration, temperature, pH value, and precipitant. In these methods, once the initial crystallization conditions are set, researchers usually try to avoid any perturbation of the protein solution, such as mechanical shock and/or temperature fluctuation. Protein crystallization in the microgravity environment of space is an ultimate idea to suppress even convection and sedimentation due to gravity, and allows for the growth of crystals *via* transport by pure diffusion.[4] In contrast to such passive crystallization methods, light has been utilized as a non-contact means for active control of crystallization. Historically, Garetz and Myerson *et al.* pioneered light-induced nucleation from supersaturated solutions in 1996.[5] They reported that nucleation of a small organic molecule (urea) could be induced by non-focused nanosecond laser irradiation, wherein the optical electric field was considered to align molecular units within clusters. It should be noted that optical absorption is not involved in the nucleation mechanism because there is no absorption at the laser wavelength, and the laser fluence (~MW cm^{-2}), which denotes laser energy per unit area, is not sufficient to cause multiphoton absorption. Thus, such a non-absorption technique was considered to be a harmless approach to crystallization. Nevertheless, in the last decade, high energy laser processing by laser ablation has shown promise for the control of protein crystallization. In contrast to the non-absorption technique, laser ablation is in general a process initiated by optical absorption of intense laser pulses that ultimately results in a change in material morphology (*e.g.*, removal of materials from a solid or liquid surface, formation of a void or bubble in the materials, *etc.*). With the recent development in pulsed lasers with ultrashort pulse widths or wavelengths (*e.g.*, femtosecond and deep-UV lasers), spatially precise, low-damage

Hiroshi Y. Yoshikawa

Hiroshi Yoshikawa received his PhD in Applied Physics from Osaka University in 2006 under the supervision of Prof. Hiroshi Masuhara. Then he joined the group of Prof. Yusuke Mori at Osaka University as a postdoctoral fellow. In 2007, he moved to the University of Heidelberg as a Humboldt fellow. Since 2011, he has been an Assistant Professor at the Department of Chemistry, Saitama University. His main scientific interests include quantitative regulation and characterization of organic molecules, polymers and cells using physico-chemical tools.

Ryota Murai

Ryota Murai received his PhD from Osaka University in 2010, under the guidance of Prof. Yusuke Mori. Afterwards he worked on protein crystallization in the same group as a postdoctoral fellow. In 2011, he joined the group of Prof. Kazuo Nakajima at Kyoto University as a postdoctoral fellow, where his research is focused on the development of a new technique to produce Si ingots for solar cells.

From right: Kazufumi Takano, Hiroaki Adachi, Shigeru Sugiyama, Tsuyoshi Inoue, Hiroyoshi Matsumura, and Yusuke Mori. Inset (left bottom): Satoshi Murakami

From right: Prof. Kazufumi Takano (Kyoto Prefectural University), Dr Hiroaki Adachi (SOSHO Inc.), Prof. Shigeru Sugiyama (Osaka University), Prof. Tsuyoshi Inoue (Osaka University), Prof. Hiroyoshi Matsumura (Osaka University), and Prof. Yusuke Mori (Osaka University). Inset (left bottom): Prof. Satoshi Murakami (Tokyo Institute of Technology). They all have been working on development of protein crystallization techniques under the interdisciplinary research project called "SOSHO project".

processing of various organic- and bio-materials has been demonstrated. For instance, femtosecond laser ablation techniques have widely been used for fine material processing including nanosurgery of cells and tissues,[6] because they can realize highly localized, low-damage processing *via* multiphoton absorption[6] and photomechanical processes.[7] In fact, the first light-induced nucleation of protein was realized by femtosecond laser processing in 2002.[8] There, protein supersaturated solutions were focused with femtosecond laser pulses with a fluence on the order of PW cm^{-2}, which is high enough to cause laser ablation of even transparent materials *via* multiphoton absorption.[8,9] Note that protein nucleation could not be induced with nanosecond laser processing, which generally causes substantial thermal damage to biological materials. To date, it has been confirmed that processing by femtosecond laser ablation can induce nucleation of various proteins at low supersaturation, thus contributing to the improvement of protein crystal quality.[10] In addition to protein nucleation, processing of protein crystals by femtosecond laser ablation can be applied to the production of single crystalline 'micro-'seeds from polycrystals and cracked crystals that are unstable for XRD studies.[11] Moreover, production of single crystalline 'macro-'seeds was achieved by deep-UV laser processing because of its potential for photochemical processes, which can reduce thermal damage to protein crystals.[12] Hence, processing by femtosecond and deep-UV laser ablation has been increasingly recognized as a promising technique for the production of protein single crystals. This review gives an overview of the successful application of femtosecond and deep-UV laser ablation to protein crystal nucleation and seeding, and also describes the advantages of laser ablation techniques from a physico-chemical perspective.

2. Femtosecond laser ablation for protein crystal nucleation

Nucleation is a first step in the crystallization process and is crucial in determining the size, shape, structure, and quality of the crystals. To induce nucleation, supersaturation should be higher than that in the "metastable" zone, where solutions are supersaturated but provide no nucleation. In general, a primary strategy for obtaining high-quality protein single crystals is to induce nucleation at supersaturation that is just above but as close as possible to the metastable zone. In fact, successful crystallization has been performed by inducing nucleation at such low supersaturation in many cases. A systematic analysis of the correlation between supersaturation and crystal quality was reported for lysozyme[13] which revealed that the crystals grown in a lower supersaturated solution diffracted better with higher signal-to-noise ratios. However, protein nucleation at low supersaturation is generally very challenging. Spontaneous nucleation rarely occurs in low supersaturated solutions (Fig. 1a, top), because the interactions between protein molecules are quite weak due to their complicated structures and large sizes.[4] In addition, the long incubation time of supersaturated solutions often denatures protein molecules in the presence of additives and/or residual protease. Therefore, crystallographers are often forced to induce protein nucleation at very high supersaturation, which results in low-quality crystals and polycrystals (Fig. 1a, bottom). In order to overcome this protein crystallization dilemma, a novel stimulus using femtosecond laser processing based on laser ablation has been utilized to induce nucleation at low supersaturation (Fig. 1b). Herein, representative proteins and small organic molecules for which nucleation can be induced by the femtosecond laser technique are reviewed, and the underlying nucleation mechanism based on laser ablation is also described.

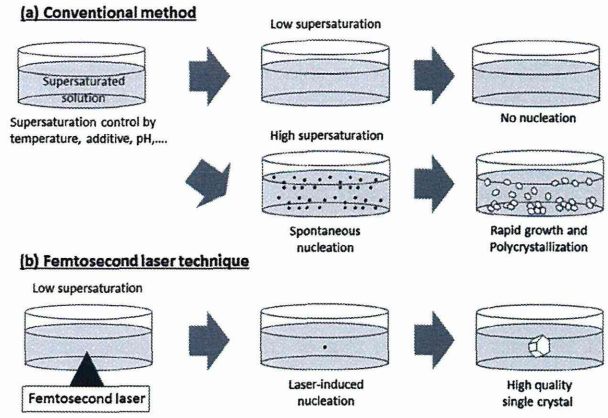

Fig. 1 Schematic illustration of crystallization processes realized by a conventional method (a) and the femtosecond laser technique (b). Reprinted with permission from SPIE, ref. 10, 2007.

Hiroshi Masuhara

Hiroshi Masuhara graduated from Tohoku University (1966) and obtained PhD degree from Osaka University (1971). He is a physical chemist working in multidisciplinary areas of photochemistry, time-resolved spectroscopy, single microparticle chemistry, single nanoparticle spectroscopy, laser ablation dynamics, and laser manipulation of single living cells. In Taiwan he is now extending seminal research studies on (1) laser trapping crystallization of molecules and proteins and (2) molecular trapping phenomena by femtosecond laser pulses. He is awarded Porter Medal and so on, and is a foreign fellow of the Royal Flemish Academy of Belgium and the National Academy of Sciences India.

2.1. Femtosecond laser-induced nucleation of proteins and small organic molecules

Adachi *et al.* demonstrated for the first time the laser-induced nucleation of proteins using a femtosecond laser.[8,9] As a first sample, they chose hen egg-white lysozyme (HEWL) (14 kDa), which has widely been used for studies of the protein crystallization mechanism. Supersaturated solutions of HEWL were

irradiated with regeneratively amplified Ti:sapphire laser (average power: 1.0 W, wavelength: 780 nm, pulse width: 120 fs, repetition rate: 1 kHz) pulses through an objective lens (numerical aperture: 0.4). They found that the number of nucleated HEWL crystals increased with the number of laser pulses. It is notable that this HEWL crystallization could not be induced by focused nanosecond laser irradiation, even though many conditions were tested (*e.g.* altering laser energy, exposure time, repetition rate, *etc.*). After the first demonstration with HEWL, the utility of the femtosecond laser technique was tested again using another model protein, glucose isomerase (GI) (tetramer; 173 kDa), having a molecular weight more than 10 times larger than that of HEWL.[9] GI crystals were also obtained by focused femtosecond laser irradiation at low supersaturation where no spontaneous nucleation occurred. This result clearly indicates that focused femtosecond laser irradiation triggered the nucleation of GI in the meta-stable zone. In addition, they found a drastic shortening of the crystallization period of *Trypanosoma brucei* prostaglandin F2α synthase (31 kDa) (TbPGFS) from several months (vapor diffusion method) to a few days (femtosecond laser technique).[9] So far, this nucleation enhancement by the femtosecond laser technique has been confirmed for a variety of proteins such as thaumatin, cytochrome *c*, and ribonuclease H (RNase H).[9,14]

Based on the success of crystallizing water-soluble proteins, the femtosecond laser technique was then applied to the crystallization of high-quality single crystals of membrane proteins, which are particularly difficult to obtain.[15] In fact, the number of membrane protein structures deposited in the PDB is only ~1400 (as of June 2013). Despite the difficulty in crystallizing membrane proteins, detailed structural information is strongly needed for the pharmaceutical sciences, where over 60% of all commercial therapeutic drugs target membrane proteins.[15] In 2004, Adachi *et al.* demonstrated nucleation of the membrane protein, AcrB,[15] which is a major multidrug efflux transporter in *Escherichia coli* and is responsible for exporting various types of antibiotics, antiseptics, anti-cancer drugs and cellular toxins from the cell.[16] AcrB supersaturated solutions with different precipitant concentrations (12, 13, and 15% of polyethylene glycol (PEG) 2000) were prepared and irradiated with focused femtosecond laser pulses (Fig. 2).

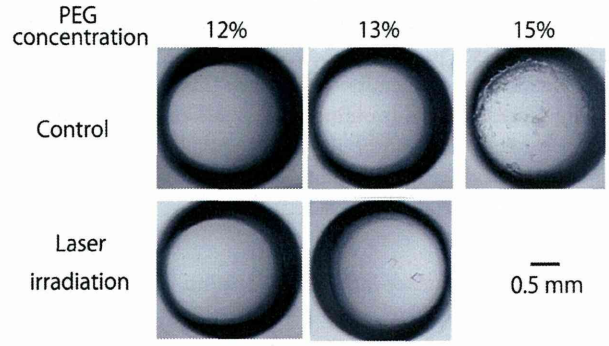

Fig. 2 Bright field images of AcrB solutions (PEG 12, 13, and 15%) irradiated without (control) and with femtosecond laser pulses. No crystallization was observed at PEG 13% without laser irradiation even after weeks. Reprinted with permission from the Japan Society of Applied Physics, ref. 15, 2004.

The images of solutions after several days clearly show that laser irradiation could induce nucleation in the meta-stable zone (13% PEG) where no nucleation occurred without laser irradiation. Large single crystals (~200 μm) were obtained from the meta-stable zone by laser irradiation, while small crystals (≤100 μm) and polycrystals were obtained by spontaneous nucleation at higher PEG concentration (15%). In addition, the AcrB crystals grown from the metastable zone diffracted to 2.3 Å resolution, which is drastically higher than that of the crystals (3.5 Å) grown from a solution with higher supersaturation (15% PEG). The femtosecond laser technique also succeeded in improving the diffraction quality and increasing the size of crystals of protein complexes including a membrane protein complex (TSecDF)[17] and a protein–RNA complex (Mnm-A-tRNA^{Glu}).[18] More recently, high-resolution structures of an enzyme (arabinanase Abnx) at 1.14 Å and its complex with a substrate (arabinobiose, DP2) at 1.04 Å were determined from single crystals grown *via* a combination of the femtosecond laser technique and a solution stirring technique.[19] A detailed study of the 3D structure at such high resolution provided new insights into the substrate-recognition mechanisms of the enzyme.

The successful protein examples clearly indicate that femtosecond laser-induced nucleation offers a viable pathway to obtaining high quality protein crystals for X-ray crystallography. Furthermore, the femtosecond laser technique can be applied not only to biological macromolecules but also to various small organic molecules.[20–24] In fact, the use of focused pulsed laser irradiation was originally proposed to induce nucleation of 4-dimethylamino-*N*-methyl-4-stilbazolium tosylate (DAST) by using a "nanosecond" laser in 2002.[25] DAST crystals are promising materials in organic nonlinear optoelectronics because of their excellent nonlinear properties. To realize high-efficiency production of high-quality DAST single crystals, nanosecond laser pulses (Nd:YAG laser, 1064 nm, 23 ns) were shot into a supersaturated methanol solution of DAST at low supersaturation. Although the efficiency of nucleation was quite low (<3%), nucleation was induced at low supersaturation where no spontaneous nucleation occurs (metastable zone). In 2005, the same research group applied focused femtosecond laser irradiation to the nucleation of DAST. They found that the efficiency of nucleation was significantly improved (~10%).[20] The next year, Yoshikawa *et al.* demonstrated femtosecond laser-induced nucleation of a water-soluble molecule, urea (Fig. 3).[21] Here, the first direct observation of crystallization dynamics initiated by focused femtosecond laser irradiation was achieved, owing to the more rapid crystallization of urea from nucleation to the formation of visibly large crystals (~mm), as compared to biological macromolecules. Another year later, Nakamura *et al.* reported the crystallization of a non-polar molecule, anthracene, from a cyclohexane solution triggered by only a single femtosecond laser pulse.[22]

Materials in which nucleation has been induced by focused femtosecond laser irradiation are listed in Table 1. The enhancement of nucleation by the femtosecond laser technique has been confirmed for various materials having widely differing properties and crystallization conditions (*e.g.*, molecular weight,

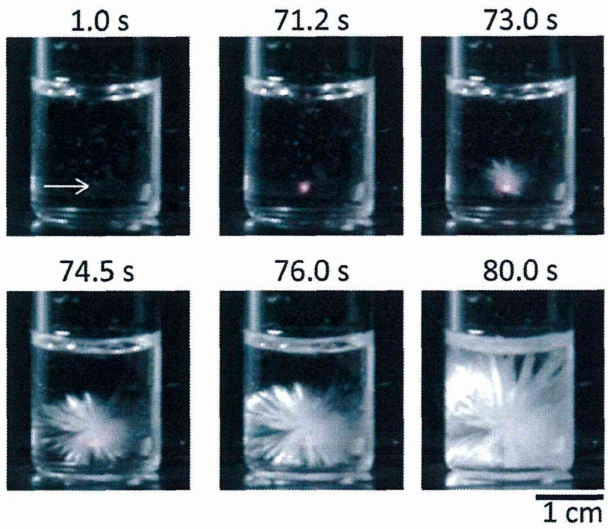

Fig. 3 Urea crystallization induced by focused femtosecond laser irradiation. The focal point of the laser pulse is indicated by an arrow in the image at 1.0 s. The delay time from the onset of laser irradiation is indicated above the images. Reprinted with permission from the Japan Society of Applied Physics, ref. 21, 2006.

solvent, additives, *etc.*). In fact, the high efficiency and versatility of the femtosecond laser technique are noteworthy compared to other light-induced crystallization techniques. For instance, Garetz *et al.* demonstrated the photophysical crystallization of urea using a non-focused nanosecond laser, wherein the optical Kerr effect organized existing prenucleating clusters, which increased the chances of nucleation and growth.[5] However, nucleation could be induced only from a supersaturated solution aged for a few days prior to laser irradiation, because the optical Kerr effect is not sufficient to reduce the entropic contribution to the free energy of activation for the induction of nucleation from a supersaturated solution in the absence of large clusters. On the other hand, the femtosecond laser technique does not require this long aging and can even induce nucleation from supersaturated solutions immediately following preparation.[21] In addition, the femtosecond laser technique can induce nucleation at 11.0 M (the solubility of urea is 10.47 M at 25 °C), while the non-focused nanosecond laser cannot below 12.0 M. As an alternative photophysical approach, the nucleation of HEWL[26] and amino acid[27] was demonstrated using radiation pressure applied by a tightly focused 1064 nm continuous wave (CW) laser. However, the solvent is limited to D_2O with this technique, because the temperature elevation due to 1064 nm photon absorption by the overtone band of the OH stretching mode in H_2O disturbs nucleation. In contrast to the CW laser approach, focused femtosecond laser irradiation can induce nucleation effectively *via* the multiphoton absorption process, which should also result in significant temperature elevation. Femtosecond lasers were typically focused into supersaturated solutions with a fluence of $\sim$PW cm^{-2}, which is extremely higher than that of a focused continuous wave (CW) laser ($\sim$MW cm^{-2}). Although most of the proteins and organic molecules mentioned above do not undergo single-photon absorption at the femtosecond laser wavelength (780–800 nm), higher order multiphoton absorption should be induced at the focal point under such intense excitation conditions. In addition, considering the versatility of the femtosecond laser technique, it seems unlikely that femtosecond laser-induced nucleation is based solely on a single, specific photochemical reaction. In the past several years, the mechanism of femtosecond laser-induced nucleation has been investigated primarily from another perspective, cavitation bubbles induced by femtosecond laser ablation, which is reviewed in the next section.

2.2. Nucleation mechanism based on femtosecond laser ablation

The first question to be answered in order to reveal the nucleation mechanism involves the identity of what is induced in protein solutions by focused femtosecond laser irradiation.

Table 1 List of materials in which nucleation can be induced by femtosecond laser ablation

	Material		Molecular weight	Solvent	Additives	Ref.
Protein	Water-soluble protein	HEWL	14.3 kDa	Water[a]	Salt	9
		Thanumatin	22 kDa		Salt	14
		RNase H	17 kDa		No additives	9
		TbPGFS	31 kDa		Salt, PEG	9
		Gl	173 kDa		Salt, PEG	9
	Membrane protein	AcrB	113.57 kDa	Water[a]	PEG, detergent	15
		TSecDF	80.5 kDa			17
	Protein complex	MnmA-tRNA^{Glu}	66 kDa	Water[a]	Salt, PEG	18
		Abnx-DP2	40 kDa		Alcohol	19
Small organic molecule	Polar molecule	Urea	60.06	Water	No additives	21
		Glycine	75.07	Water		23
		Acetaminophen	151.17	Water		24
		DAST	410.1[b]	Methanol		20
	Nonpolar molecule	Anthracene	178.23	Cyclohexane	No additives	22

[a] pH buffer solution. [b] Molecular weight of the cation–anion pair.